Journal of Metals, Materials and Minerals, Vol. 32, No. 3, pp. 118-125, 2022

Effect of A-site modification on structural and microwave dielectric properties of calcium titanate

Shailendra RAJPUT[1,2], and Sunita KESHRI[1,*]

[1] *Department of Physics, Birla Institute of Technology, Mesra, RANCHI 835215, INDIA*
[2] *Department of Physics, University Centre for Research & Development, Chandigarh University, MOHALI 140431, INDIA*

***Corresponding author e-mail:** s_keshri@bitmesra.ac.in

Received date:
1 April 2022
Revised date
13 July 2022
Accepted date:
10 August 2022

Keywords:
Perovskite structure;
Dielectric properties;
Temperature coefficient of resonant frequency

Abstract

This article presents studies on characteristics properties of $CaTiO_3$, $Ca_{0.8}Sr_{0.2}TiO_3$, and $Ca_{0.6}La_{0.8/3}TiO_3$ ceramics. These ceramics were synthesized using the solid-state reaction process. Structural examination revealed that the grown ceramics have an orthorhombic structure with the *Pbnm* space group. The random distribution of particle size was shown through morphological investigation. Apparent density of developed ceramics was determined using the Archimedes technique and found to be < 90%. The microwave dielectric properties of grown ceramics are compared on the basis of ionic polarizability. It is observed that partial replacement of Ca-ions by Sr-ions provides a high permittivity value (ε_r = 168.93), higher quality factor $Q \times f$ = 9,330 GHz), and enhanced positive temperature coefficient of resonant frequency (τ_f = 908.17). However, the substitution of Ca-ions by La-ions offers a low permittivity value (113.35), higher quality factor (16,730 GHz), and decreased temperature coefficient of resonant frequency (229.49 ppm/°C). These materials can be used with the ceramics possessing a negative temperature coefficient of resonant frequency to balance its τ_f-value nearly to zero.

1. Introduction

The continuing evolution of ceramic materials and the associated technologies are accelerating rapidly. These materials have essential roles in the wireless communication industries, which require signals of higher (microwave) frequency range and miniature circuits [1-4].

The ceramic dielectric resonators (DRs) are the most important components in microwave devices [5-7]. The DRs must have high relative permittivity (ε_r) for compact size, large quality factor ($Q \times f$) for precise frequency selectivity, and almost zero temperature coefficient of resonant frequency (τ_f) for thermal constancy [8]. Two traditional techniques for dielectric ceramic modification with desired features are known: one is to produce a new dielectric ceramic material, and the other is to make a composite utilizing two or more dielectric materials with characteristic compensation. The most common strategy is to combine two or more chemicals with negative and positive τ_f values to achieve nearly equal zero τ_f values [6,9-12]. For example, $0.95MgTiO_3 - 0.05CaTiO_3$ ceramic shows (ε_r) ~21, ($Q \times f$) ~56,000 GHz at 7 GHz and $\tau_f \sim 0$ ppm/°C [11]. Though, the sintering temperature of $MgTiO_3 - CaTiO_3$ ceramics is comparatively high (1450°C) for real-world applications.

Several other properties of $CaTiO_3$-based composites are under recent investigations. In a recent paper [13], the electrical properties, XPS-results, and impedance of $CaCu_3TiO_{12} - CaTiO_3$ have been thoroughly explained. In another paper [14], the $CaTiO_3 - LaAlO_3$ composite microwave ceramic has been used in designing dielectric patch antennas. Also, the thickness-dependent hysteresis behaviors of $CaTiO_3$ films [15] have been reported for a metal-$CaTiO_3$-metal structure which can have a potential use in the extremely low voltage. The $CaTiO_3$ is a perovskite-structured mineral that shows good microwave dielectric properties ($\varepsilon_r \sim 170$, $Q \times f \sim 3{,}600$ GHz at 7 GHz, and $\tau_f \sim 1800$ ppm/°C) [16]. The $CaTiO_3$-based materials have promising properties of ferroelectricity, piezoelectricity, elasticity, and microwave dielectric [17]. These properties have sparked great interest among researchers. In recent work, Bai *et al* showed the applicability of $CaTiO_3$ for microwave absorption in X and Ku bands [18]. The $CaTiO_3$-based ceramics have been mostly used as one component of the composite materials to get good microwave dielectric properties due to their moderate dielectric value and positive τ_f [6,11, 12,19-24]. The selection of materials for composite is essential to know its structural and microwave dielectric properties in detail. Numerous efforts have been paid to improve the microwave dielectric properties of $CaTiO_3$ ceramics [16,25-29]. A recent paper reports on the structural and microwave dielectric properties of Zr^{4+} doped $CaTiO_3$ ceramics [16]. The approach of creating a new single-phase compound with desirable dielectric properties is uncommon, although this is more important and easier for obtaining suitable microwave dielectric parameters. We have not come across any detailed reports about the single phase $Ca_{0.8}Sr_{0.2}TiO_3$ and $Ca_{0.6}La_{0.8/3}TiO_3$ ceramics in the literature.

Keeping these in mind, we have synthesized the single phase samples of $CaTiO_3$, $Ca_{0.8}Sr_{0.2}TiO_3$, and $Ca_{0.6}La_{0.8/3}TiO_3$ ceramics using solid state reaction method. The structural and microwave dielectric properties of these ceramics have been reported in this paper. The preliminary aim of this work is to achieve comparatively low positive τ_f with good combination of microwave dielectric properties so that composites with nearly zero τ_f value and higher quality factor can be achieved.

2. Experimental details

In this work, the well known solid state reaction (SSR) method was employed for sample preparation. In this work, $CaCO_3$ (99.9%, Sigma-Aldrich), TiO_2 (99%, Merck), $SrCO_3$ (99.9%, Aldrich) and La_2O_3 (99.9%, Loba Chemie) were used as starting chemicals. The starting materials were mixed according to the stoichiometric ratio for 24 h using an ordinary ball mill. The precursors were dried separately and calcined at 1100°C for 4 h with heating rate of 5°C·min^{-1}. The samples were cooled down with natural cooling. Cylindrical pellets were then made by mixing the obtained powder with 3 wt% of a 10% polyvinyl alcohol solution. This can be achieved by pressing the resulting powder into a pellet at pressure normally 8 tons to 10 tons per square inch. For $CaTiO_3$ (CT) and $Ca_{0.8}Sr_{0.2}TiO_3$ (CST), the sintering temperature was 1250°C whereas $Ca_{0.6}La_{0.8/3}TiO_3$ (CLT) was sintered at 1350°C for 4 h. The heating rate was 5°C·min^{-1} and samples were cooled down naturally. The X-ray diffraction (XRD) analysis was performed at room temperature using an X-ray diffractometer (model Bruker D8 Advance). Data were taken for the range $20^o \leq 2\theta \leq 80^o$, and the step size was 0.02. The structural analysis was performed using the Rietveld refinement technique [30] and FullProf software. The room temperature Raman spectra were captured using Raman microscopy (RENISHAW). The spectra were acquired in backscattering geometry using an argon ion laser source for the range of 100 cm^{-1} to 1000 cm^{-1}, using 2400 lines per mm grating. The excitation wavelength was 514 nm and the data point acquisition time for this job was 20 s. A scanning electron microscope (SEM, JEOL-6330F) was used for the analysis of sample morphology.

The Archimedes principle was employed to obtain the apparent density of the grown samples. Firstly, the dry weight (D) of pellet was measured using a digital electronic balance. A glass beaker with the sample immersed in distilled water was kept in a vacuum chamber for 2 h. In this process. the pores present in the pellet were completely filled with water. The weight of the pellet was again taken and interpreted as soaked weight (W). In second step, the sample was suspended in water with the help of a hanger to hang the pellet in water and the measured weight was interpreted as suspended weight (I). The apparent density $\rho_{apparent}$ was calculated using the Archimedes principle [19]:

$$\rho_{apparent} = \frac{D}{W - I} \tag{1}$$

The Hakki-Coleman dielectric resonator technique was used to determine the microwave dielectric characteristics [31]. The temperature coefficient of resonant frequency (τ_f) values were calculated as follows [4]:

$$\tau_f = \frac{f_2 - f_1}{f_1(T_2 - T_1)} \tag{2}$$

Where f_1 and f_2 are the resonant frequencies at two different temperatures T_1 (~25°C) and T_2 (~85°C), respectively.

3. Results and discussions

The XRD patterns of CT, CST, and CLT samples, taken at room temperature, are illustrated in Figure 1. The XRD analysis confirms the single phase formation of CT, CST, and CLT ceramics without additional impurity peaks. The primary study shows that the grown ceramics consist of an orthorhombic perovskite structure. The XRD patterns are indexed with the JCPDS database and observed to match well with orthorhombic structure (JCPDS card no. 89-4466). The XRD patterns of CST and CLT samples show good agreement with previous reports [32,33]. Inset shows the XRD patterns for $2\theta = 32.3$-33.5^o. As evident from Figure 1, the peaks of CST and CLT ceramics shift towards the lower angle. The relative intensities of the small peaks decrease gradually, and there are no such peaks for CLT ceramic. Such shifting of peaks indicates that the unit cell volume of CST and CLT ceramics is larger than the unit cell volume of CT, which confirms that the Sr and La substitution on Ca-site causes an upsurge in unit cell parameters and volume. The crystallite size (D) was measured using Debye Scherrer method [34-36]:

$$D = \frac{0.9\lambda}{\beta \cos\theta} \tag{3}$$

Where λ is defined as the wavelength of Cu-K_α radiation. The terms θ and β are defined as diffraction angle and the line broadening, respectively, at FWHM of the XRD, after subtracting the instrumental line broadening (in radian). The average crystallite size of CT, CST and CLT are found to be 90.39 nm, 108.49 nm and 96.73 nm, respectively. In the inset of Figure 1, there are some distinct shoulder peaks observed for CT and CST samples, however, these shoulder peaks are disappeared in case of CLT. It seems that the peaks corresponding to (112) and (020) planes of CLT ceramic have been merged.

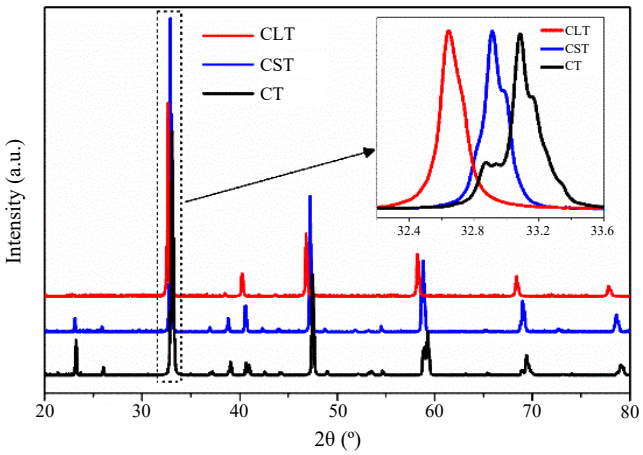

Figure 1. Room temperature XRD patterns of CT, CST and CLT ceramics. Inset shows the XRD patterns for $2\theta = 32.3°$ to $33.5°$.

The Rietveld refinement analysis was used to look into the precise description of structural properties. The refinement results of all three samples are graphically given in Figures 2(a-c). The XRD data of the CT sample were refined assuming the orthorhombic $GdFeO_3$–type structure [37], and the obtained results are demonstrated in Figure 2(a). Successful refinement confirms that the lattice structure of CT ceramic is orthorhombic with *Pbnm* space group and lattice parameters: a = 0.53869 nm, b = 0.54457 nm, and c = 0.76480 nm. The refinements have produced satisfactory *R*–factors: R_p (%) = 7.78, R_{wp} (%) = 19.3, R_{exp} (%) = 11.6 and R_{Bragg} (%) = 4.16. Figure 2(b) depicts the CST refinement findings graphically. The atomic and lattice properties of beginning member CT with the *Pbnm* space group were used in the refining procedure. The stoichiometric ratio was used to determine the occupancy factors for the mixed Ca and Sr sites.

The structural analysis confirms that the CST ceramic possesses *Pbnm* space group with an orthorhombic structure and lattice parameters are a = 0.54276 nm, b = 0.54549 nm, and c = 0.76899 nm. Figure 2(c) represents the final output after structural refinements of the CLT ceramic. The refinement is done by taking the atomic and lattice parameters of CT with the *Pbnm* space group. The Ca and La displacement parameters have been constrained to be equal. Previously, we found that the CLT structure is cubic, and the final value of R_{wp} and the goodness of fit indicator, X^2 *(=* R_{wp} */* R_{exp}*)* are 32.73 and 3.43, respectively [20]. According to the Raman spectroscopy results of CLT, we tried to perform the Rietveld refinement of CLT and found it to be best fitted as an orthorhombic phase of space group *Pbnm* with lattice parameters a = 0.54804 nm, b = 0.54929 nm, and c = 0.77512 nm (Table 1). All R- factors for the CLT system are lowered than those for the cubic structures of the system. The final weighted *R*-factors, R_{wp}, and the goodness of fit indicator, X^2 were decreased to 15.3% and 2.81%, respectively. So CLT can be fitted as cubic or orthorhombic, which may be due to the $LaTiO_3$, which has two types of structure; cubic and orthorhombic as per JCPDS card no. 84–1089 and 75–0267, respectively. But from Reitveld and Raman spectroscopy analysis, it can be concluded that CLT can be considered as an orthorhombic phase rather than a cubic. The VESTA program (v.3.0 for Windows) is employed to display unit cell structures (Figure 3).

In these figures, blue-colored portions of Ca atoms demonstrate the amount of Sr or La substitutions, respectively. Table 1 illustrates that the lattice parameters and unit cell volume are found to increase as the average A-site cation radius increases, which is in agreement with previous reports [29,37]. It is a well-known fact that the substitution of a larger ion enlarges the unit cell in all three directions. As a result, the volume of the unit cell enhances in the same space. However, no structural phase transition related to increasing A–site radius has been found in this system. It is also found that the Ti-O(1) bond length increases, and the average Ti-O(2) bond length decreases with Sr and La substitutions.

If the crystallite size is small enough to expand the XRD peaks, qualitative analysis employing XRD data is challenging (Figure 1). As a result, the use of Raman spectroscopy to confirm the phase identification of these powders was suggested. In order to determine the phase, Raman spectroscopy was adopted as a supplemental approach [38]. Four molecular units in the primitive cell, arranged in the orthorhombic structure with *Pbnm* space group, shows 24 Raman active modes. These modes are designated as: $\Gamma_{Raman,Pbnm} = 7A_g + 7B_{1g} + 5B_{2g} + 5B_{3g}$ [39,40]. Several modes cannot be detected due to low polarizability. The unpolarized Raman spectrum of CT ceramic has only nine Raman modes, as shown in Figure 4(a). The spectrum shows two broad bands at 150 cm^{-1} to 550 cm^{-1} and 550 cm^{-1} to 750 cm^{-1}. The first band comprises various sharp peaks, which are assigned to the first order Raman bands [41]. The broadness of bands is related to second order scattering. The A_g mode (158 cm^{-1}) corresponds to Ca-TiO_3 lattice mode. The modes A_g (182, 226, and 286 cm^{-1}), B_{1g} (247 cm^{-1}), and B_{3g} (337 cm^{-1}) are assigned to O-Ti-O bending modes. The modes A_g (471 cm^{-1}), B_{1g} (454.9 cm^{-1} and 495 cm^{-1}) are related to Ti-O_6 torsional modes. The spectrum of CST contains 8 Raman modes in the range of 100 cm^{-1} to 1000 cm^{-1}, as revealed from Figure 4(b). It is reported that the Raman active modes are absent in cubic structured $SrTiO_3$ with *Pm3m* space group; its spectrum consists of two strong and broad second order Raman bands situated at 200 cm^{-1} to 500 and 600 cm^{-1} to750 cm^{-1} [39]. For the CST ceramic, the O-Ti-O bending modes are observed at bands A_g(169, 209, and 282 cm^{-1}), B_{1g}(232 cm^{-1}), and B_{3g} (330.2 cm^{-1}).

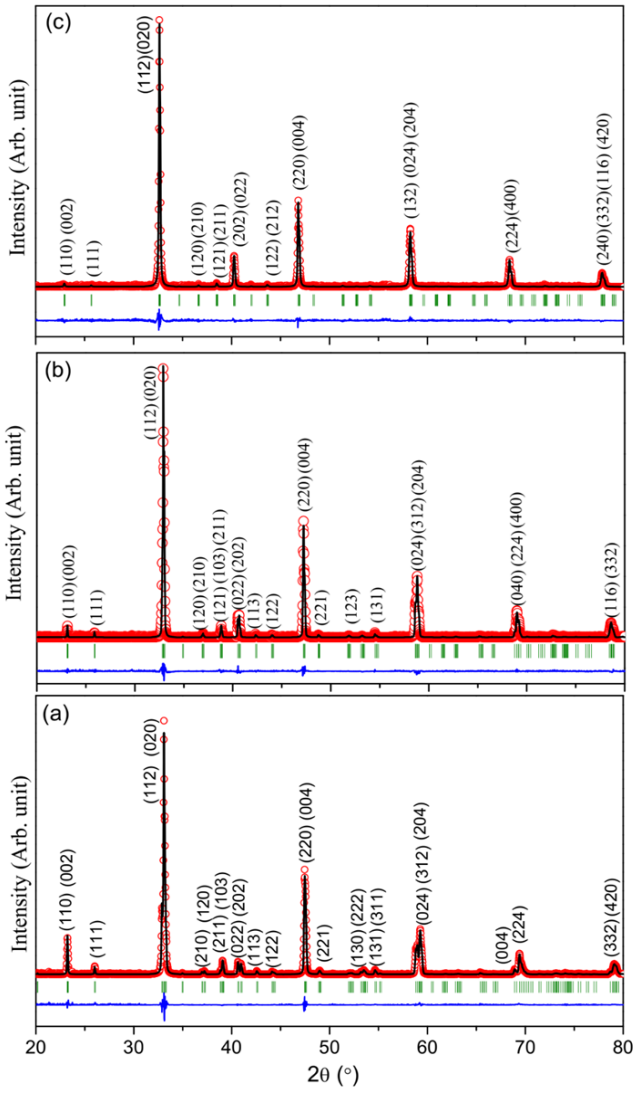

Figure 2. Rietveld refinement plots of (a) CT, (b) CST and (c) CLT. The open symbol and continuous line represent the observed and calculated intensity, respectively. The green vertical lines correspond to the positions of the computed Bragg reflections. The blue graph at the bottom represents the difference between the observed and calculated intensities.

The other bands, A_g (466.9 cm^{-1}), B_{1g} (454.9 and 488.1 cm^{-1}), are assigned to Ti-O_6 torsional modes, and all modes belong to orthorhombic structure [42]. In comparison with the bands of the CT sample at 247 cm^{-1} and 471 cm^{-1}, the corresponding bands of the CST sample shift to some lower values 232 cm^{-1} and 467 cm^{-1}. Qin *et al* have also observed similar findings [32].

It is also observed that the shifting of lower frequency modes is larger than that of the higher frequency range. The degree of crystallization, structural defects, interaction force between ions, and influence of doping ions can be responsible for observed characteristic Raman modes [43]. Figure 4(c) demonstrates that the perovskite structure of CLT consists of 8 Raman modes. The Raman band B_{2g} (115 cm^{-1}) is assigned to the Ca-TiO_3 lattice mode. The bands, A_g (163 cm^{-1} and 285 cm^{-1}), B_{1g} (219.5 cm^{-1}), and $B3_g$ (330.8 cm^{-1}), are related to O-Ti-O bending modes. The band A_g (461.2 cm^{-1}) is assigned to Ti-O_6 torsional modes. The band at 796.5 cm^{-1} is associated with B_{2g} mode. Raman bands of $LaTiO_3$ are related to bands at 399.6 cm^{-1} and 513.8 cm^{-1}. The band at 796 cm^{-1} may be linked with local vibrational modes of the La^{3+} containing complexes with different configurations. A similar type of explanation is also given in the paper of Huong *et al.* [44]

The SEM is used to investigate the morphological analyses of grown ceramics; the results are shown in the Figures 5(a-c). The grains are of various sizes, as seen in these diagrams. Different-sized grains are formed at the A–site because the diffusion rates of the two ions differ. Inhomogeneous grain sizes can be caused by the structural disorder, lattice strain caused by a change in ionic radii, and clustering in the particles integrated at the A–site. Table 2 contains the values of apparent density, theoretical density, and relative density of the samples. Theoretical density has been calculated using XRD data with the help of the Rietveld refinement method. The apparent density was determined using the Archimedes method. The ratio of these two values gives the relative density of the sample. It is found that the density of CST and CLT is higher than that of CT, which is because the atomic weights of Sr and La are higher compared to the atomic weight of Ca. From Table 2, it is evident that the relative density of grown ceramics (CT, CST, and CLT) is more than 90%.

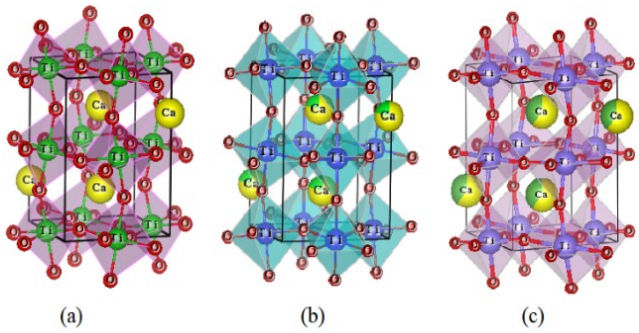

Figure 3. Schematic representation of (a) CT, (b) CST, and (c) CLT unit cells with orthorhombic structure.

Table 1. Crystallographic data of CT, CST, and CLT ceramics obtained using the Rietveld refinement method.

Sample	CT	CST	CLT
a (nm)	0.53869(1)	0.54276(2)	0.54804(3)
b (nm)	0.54457(1)	0.54549(1)	0.54929(2)
c (nm)	0.76480(2)	0.76899(2)	0.77512(4)
Z (f.u./cell)	4	4	4
Volume (nm^3)	0.22436	0.22768	0.23334
Volume/f.u. (nm^3)	0.05609	0.05692	0.05834
Structure type	Orthorhombic	Orthorhombic	Orthorhombic
Space group	*Pbnm*	*Pbnm*	*Pbnm*
$x_{(Ca/Sr/La)}$	-0.0044(6)	0.0030(13)	0.0094(11)
$y_{(Ca/Sr/La)}$	0.0288(4)	0.0219(5)	0.0157(8)
$z_{(Ca/Sr/La)}$	0.25	0.25	0.25
x_{Ti}	0.0	0.0	0.0
y_{Ti}	0.5	0.5	0.5
z_{Ti}	0.0	0.0	0.0
x_{O1}	0.0672(12)	0.0582(4)	-0.0235(7)
y_{O1}	0.4815(11)	0.4804(2)	0.5132(3)
z_{O1}	0.25	0.25	0.25
x_{O2}	0.7158(9)	0.7162(13)	0.7149(3)
y_{O2}	0.2877(8)	0.2819(13)	0.2322(9)
z_{O2}	0.0391(6)	0.0366(14)	0.0209(13)
R_{Bragg}	4.16	4.90	5.88
R_p	7.78	11.8	16.0
R_{wp}	19.3	21.0	25.6
R_{exp}	11.6	11.6	15.3
χ^2	2.78	3.29	2.81
$d_{Ti–O1}$ (nm)	0.19486	0.19512	0.19564
$d_{Ti–O2}$ (nm)	0.19735	0.19547	0.17436
$\theta_{Mn–O1–Mn}$	157.75º	160.32º	164.18º
$\theta_{Mn–O2–Mn}$	156.05º	157.76º	169.55º

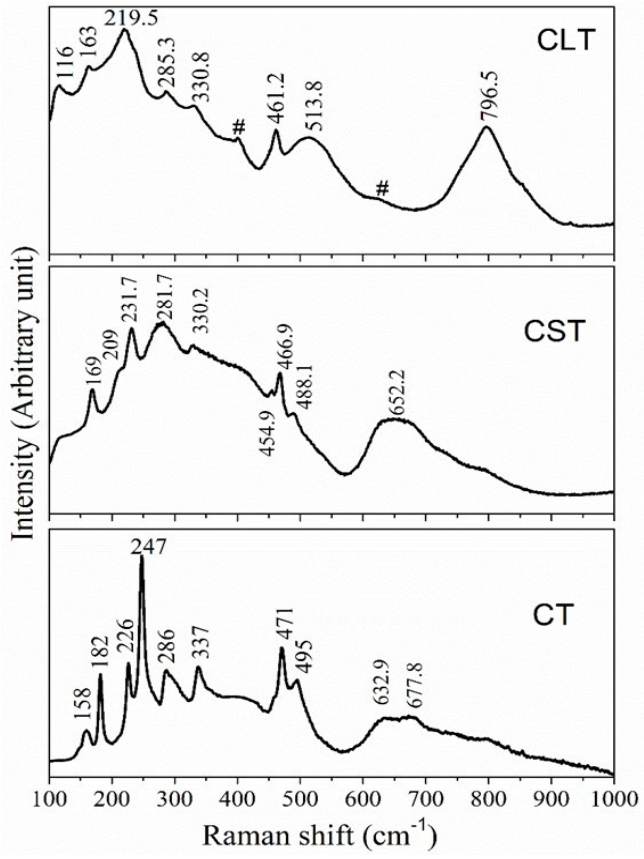

Figure 4. Raman spectra of CT, CST, and CLT ceramics.

The microwave dielectric properties of CT, CST, and CLT ceramics are listed in Table 3. The CST sample exhibits higher ε_r and high $Q \times f$ as compared to the same for CT, whereas the CLT sample shows lower ε_r and high $Q \times f$. The α_{theory} value of CST is larger than that of CT because of the greater ionic polarizability of Sr (4.24 Å) than that of Ca (3.16 Å) [29]. Hence CST ceramic shows a higher ε_r than that of CT. Due to Sr^{2+} content, a strong vibration of the atoms occurs in the lattice, resulting in enhancement of the ionic polarizability, which causes a decrease in the dielectric loss [28,45,46] and hence the $Q \times f$ value increases for CST as compared to that for CT ceramic. On the other hand, the ε_r of CLT is less as compared to CT. In the case of CLT ceramic, the La^{3+} ion is doped at Ca-site (Ca^{2+}). The charge neutrality of the structure is maintained by the formation of crystal distortions and cationic vacancies. As a result, ionic polarizability and anharmonicity associated with ion mobility tend to diminish, lowering, which decreases the dielectric constant [26,47]. The τ_f values of CT, CST, and CLT ceramics are found to be 796.69, 908.17, and 229.49 ppm/°C, respectively. It is also important to note that out of these three samples, the CST sample has the highest value of relative density and permittivity. It signifies that density has an important role in getting the permittivity value which basically defines the ability of the sample to store the electrical energy in an electric field. The temperature variation of the resonant frequency originated mainly from the temperature dependence of the ε_r. It is predicted that the τ_f behavior is related to the crystal lattice distortion, which depends on the changes in charge and size of A-site ions. Also, the τ_f values are significantly impacted by the structural phase transitions [48,49]. The distortion of the structure increases if there is symmetry loss at the structural transition, which encourages a reduction in τ_f values. The dependence of microwave dielectric parameters on the grain boundaries of the samples is not very clear in this study. We have reviewed the dielectric parameters of similar compositions and added some data in Table 3, where we find that for CT and CST we have achieved comparatively low positive τ_f and large quality factor.

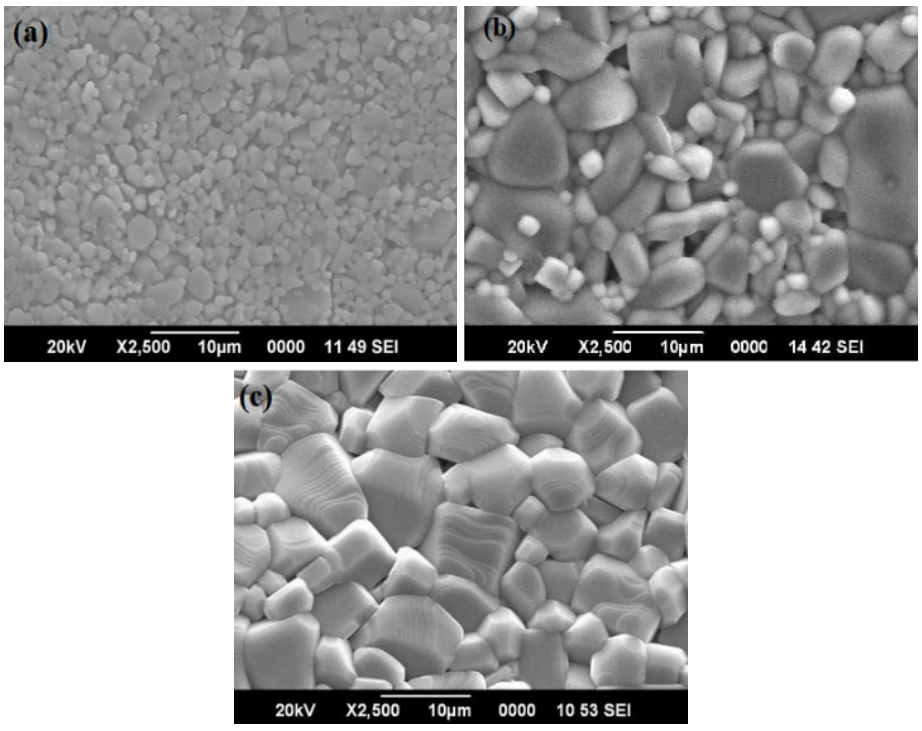

Figure 5. SEM micrographs of (a) CT, (b) CST and (c) CLT.

Table 2. Density results of CT, CST, and CLT samples.

Sample	ρ_{theory} (g·cm^{-3})	$\rho_{apparent}$ (g·cm^{-3})	$\rho_{relative}$ (%)
CT	4.026	3.859	95.852
CST	4.424	4.281	96.768
CLT	5.040	4.734	93.929

Table 3. Microwave dielectric parameters of CT, CST, and CLT samples.

Samples	ε_r	$Q \times f$ (GHz)	τ_f (ppm/°C)	
CT	145.97	4,020	796.69	This work
	170	3,600	800.12	[16]
CST	168.93	9,330	908.17	This work
	181	8,296	991	[28]
CLT	113.35	16,730	229.49	This work
	117.4	13,375	217.2	Conventional sintering [50]
	119.6	17,858	155.5	Microwave sintering [50]

4. Conclusions

Polycrystalline dielectric materials (CT, CST, and CLT with positive (τ_f) were successfully prepared by the solid-state reaction method. The crystal structures and phase formation were systematically examined using the Rietveld refinement method. The structural analysis confirms that the CT, CST, and CLT ceramics show an orthorhombic perovskite structure. The average crystallite size of CT, CST and CLT are found to be 90.39 nm, 108.49 nm and 96.73 nm, respectively. The presence of single-phase compositions is also verified by Raman analysis. Microstructural analysis of grown ceramics demonstrates well defined grains and grain boundaries with 90% relative density. A standard Hakki-Coleman method was used to measure microwave dielectric properties. Changes in ionic polarizability, electronic polarizability, and A-site substitutions are linked to dielectric characteristics. The CST ceramic exhibits higher ε_r (168.93) and $Q \times f$ (9,330 GHz) values, whereas the CLT sample shows lower ε_r (113.35) and higher $Q \times f$ (16,730 GHz), as compared to the same for CT ($\varepsilon_r \sim$145.97, $Q \times f$ ~4,020 GHz). Substitution of Sr ion at Ca-site gives an enhanced positive τ_f value (908.17 ppm/°C), whereas La substitution provides decreased positive τ_f value (229.49 ppm/°C) than that of pure $CaTiO_3$ (796.69 ppm/°C). The CST sample has the highest value of relative density and permittivity, signifying that it can store more electrical energy compared to other two, in the presence of an electric field. It is important to note that the CLT sample shows the comparatively low positive τ_f value with higher quality factor. It can be mixed with ceramics of negative τ_f value (*e. g*. $MgTiO_3$-based ceramics) in order to get nearly zero τ_f values with good combination of microwave dielectric properties. Such composites can be used in dielectric resonator antenna (DRA), which are useful for different fields of microwave communication.

Acknowledgements

The authors are thankful to the members of Central Instrumentation Facility Lab, Birla Institute of Technology, Mesra for providing SEM and EDX facilities.

Conflict of interest

The authors declare no financial or commercial conflict of interest.

References

[1] W. Lou, M. Mao, K. Song, K. Xu, B. Liu, W. Li, B. Yang, Z. Qi, J. Zhao, S. Sun, H. Lin, Y. Hu, D. Zhou, D. Wang, and I. M. Reaney, "Low permittivity cordierite-based microwave dielectric ceramics for 5G/6G telecommunications," *Journal of the European Ceramic Society,* vol. 42, pp. 2820-2826, 2022.

[2] H. Lim and Y.-J. Oh, "Low-temperature sintered Bi1-xSmxNbO$_4$ microwave dielectrics," *Journal of the European Ceramic Society,* vol. 40, pp. 1191-1197, 2020.

[3] D. Wang, L. Li, J. Jiang, Z. Lu, G. Wang, K. Song, D. Zhou, and I. M. Reaney, "Cold sintering of microwave dielectric ceramics and devices," *Journal of Materials Research,* vol. 36, pp. 333-349, 2021.

[4] S. S. Rajput and S. Keshri, "Structural and microwave properties of (Mg,Zn/Co)TiO$_3$ dielectric ceramics," *Journal of materials engineering and performance,* vol. 23, pp. 2103-2109, 2014.

[5] M. T. Sebastian, *Dielectric materials for wireless communication*: Elsevier, 2010.

[6] S. S. Rajput, S. Keshri, V. R. Gupta, N. Gupta, V. Bovtun, and J. Petzelt, "Design of microwave dielectric resonator antenna using MZTO–CSTO composite," *Ceramics International,* vol. 38, pp. 2355-2362, 2012.

[7] R. K. Bhuyan, "Ultra-low loss Mg_2TiO_4 based dielectric ceramics for microwave applications: An Overview," *Micro and Nanosystems,* vol. 14, pp. 110-120, 2022.

[8] J. Lv, Z. Cao, Y. Wang, F. Shi, and J. Wang, "Crystal structures and microwave dielectric properties of Sr_2MgWO_6 ceramics at different sintering temperatures," *Journal of Materiomics,* vol. 8, pp. 79-87, 2022.

[9] L. He and R. Zuo, "A novel (1-*x*)$MgZr_{0.85}Sn_{0.15}Nb_2O_8$-*x*$Ba_3Ti_4Nb_4O_{21}$ microwave dielectric composite ceramic with near-zero temperature coefficient," *Journal of Alloys and Compounds,* vol. 896, p. 163101, 2022.

[10] Y. Yu, Y. Wang, W. Guo, C. Zhu, A. Ji, H. Wu, *et al.*, "Grain size engineered $0.95MgTiO_3$–$0.05CaTiO_3$ ceramics with excellent microwave dielectric properties and prominent mechanical performance," *Journal of the American Ceramic Society,* vol. 105, pp. 299-307, 2022.

[11] Y.-C. Chen, S.-M. Tsao, C.-S. Lin, S.-C. Wang, and Y.-H. Chien, "Microwave dielectric properties of $0.95MgTiO_3$–$0.05CaTiO_3$ for application in dielectric resonator antenna," *Journal of Alloys and Compounds,* vol. 471, pp. 347-351, 2009.

[12] R. G. M. Oliveira, R. A. Silva, J. E. V. De Morais, G. S. Batista, M. A. S. Silva, J. C. Goes, H. D. de Andrade, I. S. Queiroz, C. Singh, A. S. B. Sombra, "Effects of $CaTiO_3$ addition on the microwave dielectric properties and antenna properties of $BiVO_4$ ceramics," *Composites Part B: Engineering,* vol. 175, p. 107122, 2019.

[13] Y. Guo, J. Tan, and J. Zhao, "Influence of CTO additives on microstructure and electrical properties of CCTO ceramics," *Materials Chemistry and Physics,* vol. 278, p. 125659, 2022.

[14] C. Du, D. Zhou, R. T. Li, H. T. Chen, G. H. Zhou, B. Tang, M. A. Darwish, S. X, and Z. Xu, "Fabrication of wideband low-profile dielectric patch antennas from temperature stable $0.65CaTiO_3$–$0.35LaAlO_3$ microwave dielectric ceramic," *Advanced Electronic Materials,* vol. 8, no. 9, p. 2101414, 2022.

[15] S. Lee, S. Kwak, T. Park, B. Son, H. J. Yun, J. Hur, and H. Yoo, "Synthesis of lead-free $caTiO_3$ oxide perovskite film through solution combustion method and its thickness-dependent hysteresis behaviors within 100 mV operation," *Molecules,* vol. 26, p. 5446, 2021.

[16] A. Zaman, S. Uddin, N. Mehboob, A. Ali, A. Ahmad, and K. Bashir, "Effect of Zr^{4+} on the structural and microwave dielectric properties of $CaTiO_3$ ceramics," *Ferroelectrics,* vol. 577, pp. 143-152, 2021.

[17] T. Křenek, T. Kovářík, J. Pola, T. Stich, and D. Docheva, "Nano and micro-forms of calcium titanate: synthesis, properties and application," *Open Ceramics,* vol. 8, p. 100177, 2021.

[18] J. Bai, W. K. Abdelbasset, S. M. Elkholi, K. A. Ismail, and M. N. Akhtar, "Efficient single and bi-layer absorbers of $CaTiO_3$ micro-cubes and polypyrrole nanotubes composites for enhanced microwave absorption in X and Ku band," *Ceramics International,* 2022.

[19] S. S. Rajput, and S. Keshri, "Structural, vibrational and microwave dielectric properties of $(1-x)Mg_{0.95}Co_{0.05}TiO_3$–$(x)Ca_{0.8}Sr_{0.2}TiO_3$ ceramic composites," *Journal of alloys and compounds,* vol. 581, pp. 223-229, 2013.

[20] S. S. Rajput, S. Keshri, and V. R. Gupta, "Microwave dielectric properties of $(1-x)Mg_{0.95}Zn_{0.05}TiO_3$–$(x)Ca_{0.6}La_{0.8/3}TiO_3$ ceramic composites," *Journal of alloys and compounds,* vol. 552, pp. 219-226, 2013.

[21] Y. Zhang, X. Jiang, S. Ding, and T. Song, "Microwave dielectric property adjustment of $CoZrNb_2O_8$ ceramics by $CaTiO_3$ addition," *Journal of Materials Science: Materials in Electronics,* vol. 32, pp. 12661-12670, 2021.

[22] Y.-C. Chen, H.-X. Liu, C.-H. Li, J.-Y. Fu, and Y.-C. Cheng, "Influence of $Ca_{0.8}Sr_{0.2}TiO_3$ on the microstructures and microwave dielectric properties of $Nd_{0.96}Yb_{0.04}(Mg_{0.5}Sn_{0.5})O_3$ Ceramics," *Ferroelectrics Letters Section,* vol. 42, pp. 1-9, 2015.

[23] C. H. Shen, C. L. Pan, S. H. Lin, W. C. Lin, and S. K. Huang, "Low-fire processing $(1-x)Mg_{0.95}Co_{0.05}TiO_3$-$xCa_{0.6}La_{0.8/3}TiO_3$ microwave dielectric ceramics," in *Applied Mechanics and Materials*, 2014, pp. 14-17.

[24] K. Yan, M. Fujii, T. Karaki, and M. Adachi, "Microwave dielectric properties of $Ca_{0.8}Sr_{0.2}TiO_3$–$Li_{0.5}Nd_{0.5}TiO_3$ ceramics with near-Zero temperature coefficient of resonant frequency," *Japanese Journal of Applied Physics,* vol. 46, p. 7105, 2007.

[25] M. Saleem, Y. Iqbal, S. Qin, X. Wu, R. Muhammad, and F. Zhu, "Structural phase transition and microwave dielectric properties of $Ca_{1-x}Sr_xTiO_3$ (x= 0.1–0.9) ceramics," *Journal of Materials Science: Materials in Electronics,* vol. 26, pp. 1507-1511, 2015.

[26] W. S. Kim, K. H. Yoon, and E. S. Kim, "Microwave dielectric properties and far-infrared reflectivity characteristics of the $CaTiO_3$–$Li_{(1/2)-3x}Sm_{(1/2)+x}TiO_3$ ceramics," *Journal of the American Ceramic Society,* vol. 83, pp. 2327-2329, 2000.

[27] R. Kell, A. Greenham, and G. Olds, "High-permittivity temperature-stable ceramic dielectrics with low microwave loss," *Journal of the American Ceramic Society,* vol. 56, pp. 352-354, 1973.

[28] P. Wise, I. Reaney, W. Lee, T. Price, D. Iddles, and D. Cannell, "Structure–microwave property relations in $(Sr_xCa_{(1-x)})_{n+1}TinO_{3n+1}$," *Journal of the European Ceramic Society,* vol. 21, pp. 1723-1726, 2001.

[29] C.-L. Huang, J.-T. Tsai, and Y.-B. Chen, "Dielectric properties of $(1-y)Ca_{1-x}La_{2x/3}TiO_3$-$y(Li,Nd)_{1/2}TiO_3$ ceramic system at microwave frequency," *Materials research bulletin,* vol. 36, pp. 547-556, 2001.

[30] H. M. Rietveld, "The rietveld method," *Physica Scripta,* vol. 89, p. 098002, 2014.

[31] B. Hakki, and P. D. Coleman, "A dielectric resonator method of measuring inductive capacities in the millimeter range," *IRE Transactions on Microwave Theory and Techniques,* vol. 8, pp. 402-410, 1960.

[32] S. Qin, X. Wu, F. Seifert, and A. I. Becerro, "Micro-Raman study of perovskites in the $CaTiO_3$–$SrTiO_3$ system," *Journal of the Chemical Society, Dalton Transactions,* pp. 3751-3755, 2002.

[33] R. Li, Q. Tang, S. Yin, and T. Sato, "Performance of $Ca_{1-x}Sr_xTiO_3$ as barriers in dielectric barrier discharges with different Sr content," *Journal of Physics D: Applied Physics,* vol. 40, p. 5187, 2007.

[34] M. Ahmadipour, M. J. Abu, M. F. Ab Rahman, M. F. Ain, and Z. A. Ahmad, "Assessment of crystallite size and strain of $CaCu_3Ti_4O_{12}$ prepared via conventional solid-state reaction," *Micro & Nano Letters,* vol. 11, pp. 147-150, 2016.

[35] M. Ahmadipour, M. Arjmand, A. T. Le, S. L. Chiam, Z. A. Ahmad, and S.-Y. Pung, "Effects of multiwall carbon nanotubes on dielectric and mechanical properties of $CaCu_3Ti_4O_{12}$ composite," *Ceramics International,* vol. 46, pp. 20313-20319, 2020.

[36] M. Ahmadipour, M. Arjmand, M. F. Ain, Z. A. Ahmad, and S.-Y. Pung, "Effect of WO_3 loading on structural, electrical and dielectric properties of $CaCu_3Ti_4O_{12}$ ceramic composites," *Journal of Materials Science: Materials in Electronics,* vol. 30, pp. 6806-6810, 2019.

[37] S. Sasaki, C. T. Prewitt, J. D. Bass, and W. Schulze, "Orthorhombic perovskite $CaTiO_3$ and $CdTiO_3$: structure and space group," *Acta Crystallographica Section C: Crystal Structure Communications,* vol. 43, pp. 1668-1674, 1987.

[38] Y.-I. Kim, J. K. Jung, and K.-S. Ryu, "Structural study of nano $BaTiO_3$ powder by Rietveld refinement," *Materials Research Bulletin,* vol. 39, pp. 1045-1053, 2004.

[39] U. t. Balachandran, and N. Eror, "Laser-induced Raman scattering in calcium titanate," *Solid State Communications,* vol. 44, pp. 815-818, 1982.

[40] P. Gillet, F. Guyot, G. D. Price, B. Tournerie, and A. Le Cleach, "Phase changes and thermodynamic properties of $CaTiO_3$. Spectroscopic data, vibrational modelling and some insights on the properties of $MgSiO_3$ perovskite," *Physics and Chemistry of Minerals,* vol. 20, pp. 159-170, 1993.

[41] P. McMillan, and N. Ross, "The Raman spectra of several orthorhombic calcium oxide perovskites," *Physics and Chemistry of Minerals,* vol. 16, pp. 21-28, 1988.

[42] T. Hirata, K. Ishioka, and M. Kitajima, "Vibrational spectroscopy and X-ray diffraction of perovskite compounds $Sr_{1-x}M_xTiO_3$ (M = Ca, Mg; $0 \leq x \leq 1$)," *Journal of solid state chemistry,* vol. 124, pp. 353-359, 1996.

[43] V. Marques, L. Cavalcante, J. Sczancoski, E. Paris, J. Teixeira, J. A. Varela, F. S. De Vicente, M. R. Jopa, P. S. Pizani, M. S. Li, M. R. M. Santos, and E. Longo, "Synthesis of $(Ca,Nd)TiO_3$ powders by complex polymerization, rietveld refinement and optical properties," *Spectrochimica Acta Part A: Molecular and Biomolecular Spectroscopy,* vol. 74, pp. 1050-1059, 2009.

[44] D. T. M. Huong, N. H. Nam, and N. N. Long, "Preparation and optical characterization of Eu^{3+}-doped $CaTiO_3$ perovskite powders," *Journal of alloys and compounds,* vol. 537, pp. 54-59, 2012.

[45] B. Lewis, "Energy loss processes in ferroelectric ceramics," *Proceedings of the Physical Society (1958-1967),* vol. 73, p. 17, 1959.

[46] H.-J. Hagemann, "Loss mechanisms and domain stabilisation in doped $BaTiO_3$," *Journal of Physics C: Solid State Physics,* vol. 11, p. 3333, 1978.

[47] A. Bisen, A. Satapathy, S. Parida, E. Sinha, S. Rout, and M. Kar, "Structural, optical band gap, microwave dielectric properties and dielectric resonant antenna studies of $Ba_{(1-x)}La_{(2x/3)}ZrO_3$ ($0 \leqslant x \leqslant 0.1$) ceramics," *Journal of alloys and compounds,* vol. 615, pp. 1006-1012, 2014.

[48] R. Lowndes, F. Azough, R. Cernik, and R. Freer, "Structures and microwave dielectric properties of $Ca_{(1-x)}Nd_{2x/3}TiO_3$ ceramics," *Journal of the European Ceramic Society,* vol. 32, pp. 3791-3799, 2012.

[49] S. Parida, S. Rout, N. Gupta, and V. Gupta, "Solubility limits and microwave dielectric properties of $Ca(Zr_xTi_{1-x})O_3$ solid solution," *Journal of alloys and compounds,* vol. 546, pp. 216-223, 2013.

[50] J.-m. Li and T. Qiu, "Microwave sintering of $Ca_{0.6}La_{0.2667}TiO_3$ microwave dielectric ceramics," *International Journal of Minerals, Metallurgy, and Materials,* vol. 19, pp. 245-251, 2012.